Wave Turbulence in Superfluid ^{4}He: Energy Cascades & Rogue Waves in the Laboratory

V. B. Efimov[*,†], A. N. Ganshin[*], G. V. Kolmakov[†,**], P. V. E. McClintock[*]
and L. P. Mezhov-Deglin[†]

[*]Department of Physics, Lancaster University, Lancaster, LA1 4YB, UK
[†]Institute of Solid State Physics RAS, Chernogolovka, Moscow region, 142432, Russia
[**]Currently at the Department of Chemical and Petroleum Engineering,
Pittsburgh University, Pittsburgh, PA 15261, USA.

Abstract. Recent work on second sound acoustic turbulence in superfluid ^{4}He is reviewed. Observations of forward and inverse energy cascades are described. The onset of the inverse cascade occurs above a critical driving energy and it is accompanied by giant waves that constitute an acoustic analogue of the rogue waves that occasionally appear on the surface of the ocean. The theory of the phenomenon is outlined and shown to be in good agreement with the experiments.

Keywords: Wave turbulence, superfluid helium, energy cascade
PACS: 52.35.Mw, 67.25.dt, 47.27.-i, 47.20.Ky

INTRODUCTION

Turbulence is all around us. The term is used to describe a highly excited state of a system with numerous degrees of freedom, characterized by a directional energy flux through frequency scales [1, 2]. In addition to the familiar manifestations of vortex turbulence in bulk fluids, sketched and discussed by Leonardo da Vinci [3, 4], turbulence can also occur in systems of waves. Examples include phonon turbulence in solids [5], turbulence of sound waves in oceanic waveguides [6], magnetic turbulence in interstellar gases [7], and shock waves in the solar wind and their coupling with Earth's magnetosphere [8]. There is usually a cascade-like transfer of turbulent energy towards the high frequency domain [2, 9], which is where dissipation mainly occurs as the result of viscous damping.

In this paper, we review recent experiments on second sound (temperature/entropy) waves in superfluid ^{4}He showing [10] that, contrary to the conventional wisdom, wave energy can also flow in the opposite direction, leading to formation of the acoustic analogue of the oceanic giant waves that sometimes endanger large ships. Experiments on giant waves are almost impossible, because they probably require hundreds of miles of open sea to build up and decay. As we will see, however, second sound is an ideal modeling medium for studies of the nonlinear wave interactions believed to be involved in the generating mechanism [11], enabling the fundamental ideas to be tested in the laboratory under controlled conditions.

We have found that in He II, in addition to the energy flux towards higher frequencies [9], a flux of energy towards lower frequencies can occur under special conditions, coexisting with the direct cascade. This backflow appears to be attributable to a decay

53

instability, i.e. nonlinear decay of the wave into two waves of lower frequency governed by the conservation law [2]

$$\omega_1 = \omega_2 + \omega_3. \tag{1}$$

where $\omega_i = u_{20}k_i$ is the frequency of a linear wave of wave vector k_i and u_{20} is the second sound velocity at vanishingly small amplitude. The instability results in the creation of subharmonics and can produce a substantial increase of low-frequency wave amplitude. A similar parametric process, but caused by 4-wave processes (modulation instability), is thought [11] to be responsible for the conversion of the energy in ordinary wind-driven waves on the ocean to take the form of rogue waves; this mechanism differs from an alternative explanation proposed recently [12] involving the scattering of nonlinear waves on a continuous noisy background. Comparable decay instabilities have been studied for e.g. spin waves [13, 14, 15], magnetohydrodynamic waves in plasma [16], and interacting first and second sound waves in superfluid helium near the superfluid transition [17].

In what follows, we introduce the relevant features of superfluid helium for non-experts, discuss how the experiments are performed, and review results obtained under both stationary and nonstationary conditions. We then provide a theoretical discussion of the observations and draw tentative conclusions.

Superfluid helium

When cooled below $T_\lambda = 2.17\,\mathrm{K}$, liquid ^{4}He enters a new state known as He II, characterised by a manifold of strange and unexpected properties [18]. In particular, it then behaves as though it were a mixture of two different fluids: a normal fluid component with viscosity and carrying all of the thermal energy of the liquid; and an inviscid superfluid component with zero entropy. Oscillatory counterflow of the two components at constant density corresponds to the temperature wave known as second sound.

Second sound has a relatively low phase velocity ($\sim$20 ms^{-1}) and an extremely low attenuation coefficient for frequencies below about 1 MHz. Its velocity u_2 depends strongly on its amplitude δT and can be approximated as

$$u_2 = u_{20}(1 + \alpha\delta T), \tag{2}$$

where the nonlinearity coefficient α [19], that determines the strength of the wave interactions, can be made large, and either positive or negative, by adjustment of the temperature. These properties make He II an ideal medium for systematic studies of nonlinear interactions between waves.

EXPERIMENTS

The experimental arrangements [9, 20] are shown schematically in Fig. 1. The cryoacoustical resonator consisted of a cylindrical quartz tube of length $L = 7$ cm and inner diameter $D = 1.5$ cm, filled with superfluid helium. The film heater and bolometer were
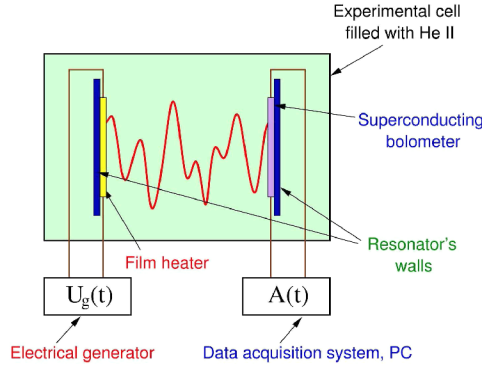
FIGURE 1.   Schematic diagram to illustrate the experimental arrangements.

deposited on the surfaces of flat glass plates capping the ends of the tube. The heater was driven by a harmonic voltage generator in the frequency range 0.1 – 100 kHz. The frequency of the second sound (twice the frequency of the voltage generator) was set close to a longitudinal resonance. The amplitude δT of the standing wave could be varied between 0.05 mK and a few mK. The temperature was maintained at $T \approx 2.08$ K, for which $\alpha \approx -7.7$ K^{-1}. The resonator's Q-factor, determined from the widths of longitudinal resonances at small heat flux densities (linear regime), was $Q \sim 3000$ for resonant numbers $30 < n < 100$. Use of a high-Q resonator enables us to create nonlinear second sound standing waves of high amplitude accompanied by only small heat input at the source, thus avoiding possible complications [21] due to vortex creation in the bulk He II and nonlinear phenomena at the heater/superfluid interface. The second sound wave shape registered by the bolometer was Fourier-analysed and its power spectrum was computed.

Stationary states

Fig. 2 presents typical results obtained when driving at a relatively high resonant frequency ω_d (the 96th longitudinal resonance of the cell). Those in Figs. 2a,b reproduce our earlier observation of the direct Kolmogorov-like cascade of second sound waves in He II [9], when driving close to resonance. Figs. 2c–f show the evolution of the wave shape and spectrum with changing the detuning of the drive frequency. Of particular interest for what follows, tiny shifts in driving frequency result in marked changes in the shape and power spectrum of the standing wave. The formation of spectral peaks near $\frac{1}{2}$, $\frac{1}{3}$ and $\frac{2}{3} \times \omega_d$ satisfy (1) with $\omega_1 = \omega_d$, supporting our inference that the instability is controlled mainly by 3-wave interactions. Huge distortions of an initially periodic signal occur as the driving frequency changes, as shown in Fig. 2c,e: when the instability develops, the signal remains nearly periodic, but its characteristic period becomes considerably longer than the fundamental period of the driving force. The amplitude of the lower-frequency waves can reach more than twice that at the driving
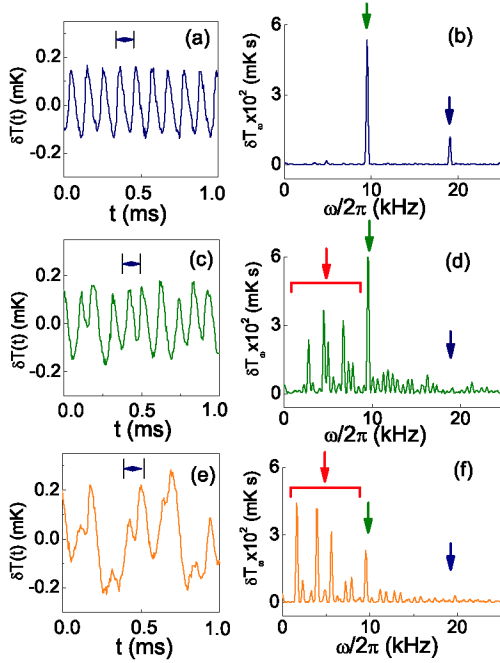
55

FIGURE 2. Evolution of the observed wave shape in the resonator (left column) and of the power spectrum of second sound standing waves (right) with increasing (small) positive detuning of the drive frequency ω_d near the 96th resonance: $\omega_d/2\pi = 9530.8$ Hz (a),(b), 9532.4 Hz (c),(d), and 9535.2 Hz (e),(f). The AC heat flux density was $W = 42$ mW/cm^2. The temperature $T = 2.08$ K corresponded to negative nonlinearity. The fundamental and first harmonic in (b),(d),(f) are indicated by vertical (green and blue) arrows; the low-frequency domain where the subharmonics appear are indicated by the horizontal ranges in (d),(f) with vertical (red) arrows. The horizontal arrows in (a),(c),(e) indicate the fundamental period of a wave at the driving frequency.

frequency.

To characterise the instability quantitatively, we use the energy contained in the low-frequency part of the spectrum $\omega < \omega_d$,

$$E_{LF} = \frac{1}{2} \left(\frac{\partial C}{\partial T} \right) \sum_{\omega < \omega_d} |\delta T_\omega|^2, \qquad (3)$$

as an indicator. For small W we did not observe any subharmonic generation at all [9]; then, above a critical flux W_c, E_{LF} rose rapidly [10], as shown in Fig. 3, suggesting that the phenomenon is of a threshold character. At $T = T_\alpha = 1.88$ K for which α vanishes [19], no subharmonics were observed, regardless of the magnitude of W, thus confirming the crucial importance of nonlinearity. For W above 10.4 mW/cm^2, we observed a distortion of the signal similar to that shown in Fig. 2c and the formation of a few subharmonics. Further increase of W above 20 mW/cm^2 led to the generation
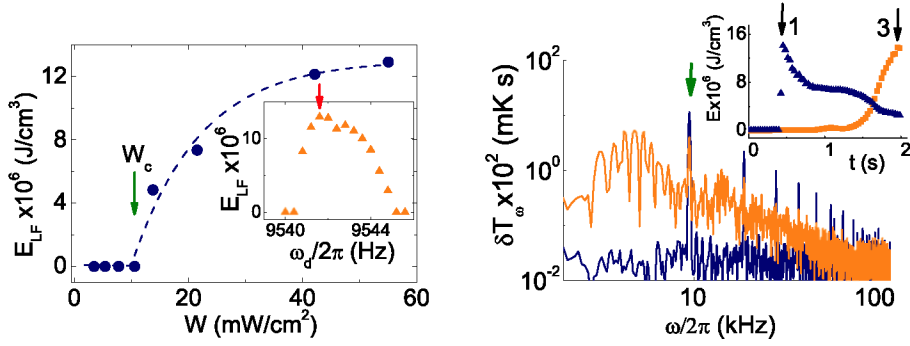
56

FIGURE 3. **Left**: The energy E_{LF} contained in the low-frequency part of the spectrum as a function of the AC heat flux density W, while driving near to the 96th resonance for $T \simeq 2.08$ K. The threshold value of W, marked by the (green) arrow, was $W_c = 10.4$ mW/cm^2. The points are from experiment; dashed lines are guides to the eye. Inset: the dependence of E_{LF} on ω_d, measured for $W = 55.6$ mW/cm^2; the (red) arrow labels the maximum value of E_{LF}, which is taken to the main figure. **Right**: Instantaneous spectra in frames 1 and 3 of Fig. 5. The lower (blue) spectrum, for frame 1, shows the direct cascade only; the upper (orange) spectrum, for frame 3, shows both the direct and inverse cascades. The (green) arrow indicates the the fundamental peak at the driving frequency. Inset: evolution of the wave energy in the low-frequency and high frequency domains is shown by the (orange) squares and (blue) triangles respectively; (black) arrows mark the positions of frames 1 and 3. From [10]

of multiple subharmonics. These phenomena appear in the regime where the energy cascade towards the high frequency domain (i.e. direct cascade, with a Kolmogorov-like spectrum [9, 22]), is already well-developed.

It is also of interest to study the response to a driving waveform more complex than the simple sinusoid discussed above. We have therefore investigated the result of applying
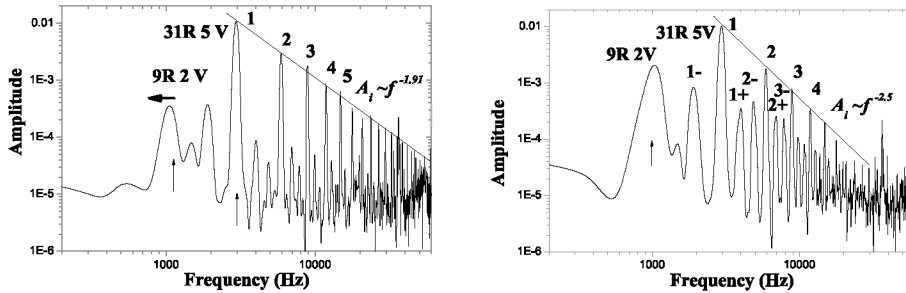

FIGURE 4. Formation of combination frequencies and suppression of the direct cascade due to pumping the resonator with an additional harmonic perturbation. $T = 2.08$ K. The main driving force of $U_{1G} = 5$ V), applied on the 31st resonance, creates a developed cascade. The additional drive of $U_{2D} = 2$ V, is applied on the 9th resonance (right panel) or detuned well away from it (left panel).
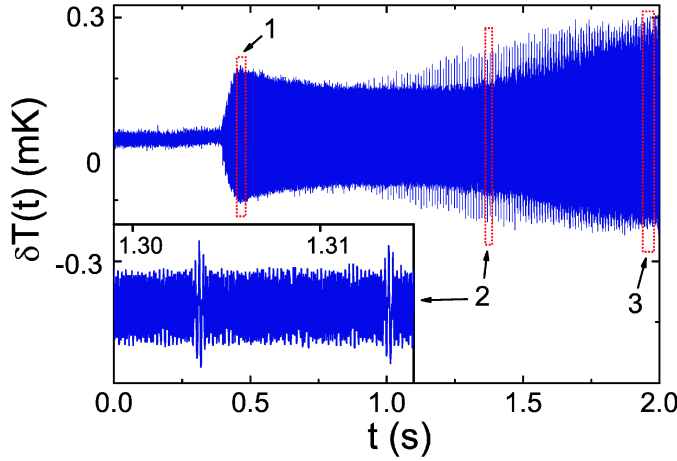
57

FIGURE 5. Transient evolution of the 2nd sound wave amplitude δT after a step-like shift of the driving frequency to the 96th resonance at time $t = 0.397$ s. Signals in frames 1 and 3 are similar to those obtained in steady-state measurements, Fig. 2 (a) and (e) respectively. Formation of isolated "rogue" waves are clearly evident. Inset: examples of isolated rogue waves, enlarged from frame 2. From [10]

a weak secondary drive at a different frequency, in addition to the main driving force. The result [23] is a marked decrease in the energy at high frequencies. It seems that this effect can arise in two ways. One of these is that the turbulent energy travels faster and more easily towards the high frequency domain where dissipation occurs. Secondly, and in addition, under appropriate conditions the additional drive triggers the onset of the inverse cascade. An example is shown in Fig. 4: two harmonic voltage generators were used, one providing the main drive of $W = 25$ mW/cm^2 on the 31st resonance, producing a developed direct energy cascade; the other applied the perturbing force of $W = 4$ mW/cm^2 near the 9th resonance, either detuned from it (left section) or on-resonance (right). When applied on-resonance, the effect of the perturbation was to mix the frequencies of both signals $2\omega_{G1}$, $\omega_{G2} - \omega_{G1}$, $\omega_{G2} + \omega_{G1}$ and $2\omega_{G2}$ and to produce combination harmonics of the main spectrum. A redistribution of energy occurred between all modes, together with an attenuation of the main energy spectrum and a change in magnitude of its negative power law exponent from ∼1.9 to ∼2.5.

Transient processes

The above results all correspond to steady-state regimes of the wave system. In Figs. 3 (right) and 5 we illustrate the *transient* processes observed after a step-like shift of the driving frequency from a frequency initially set far from any resonance to the

58

96th resonance frequency for $W = 42.1\,\text{mW/cm}^2$, $T = 2.08$ K. We find that harmonics of the drive in the high-frequency spectral domain are formed very quickly, but that formation of the subharmonics takes much longer: it took ~ 0.5 s here, and can reach several tens of seconds under some conditions [10]. It is evident from the inset in Fig. 5 that, as the instability develops, isolated "rogue waves" appear in the signal. As time evolves, the rogue waves appear more frequently and, at the later stages, they merge resulting in the strong low-frequency modulation of the signal observed in the steady-state measurements (Fig. 2).

When the subharmonics appear, a marked reduction occurs in the energy contained in the high-frequency spectral domain [10]. Much of the energy injected at the driving frequency ω_d then flows towards the low frequency domain $\omega < \omega_d$ leading to an accumulation of wave energy there, with a corresponding increase in wave amplitude. The reduction of wave amplitude seen in the high frequency spectral domain clearly indicates the onset of energy backflow towards lower frequencies, i.e. a sharing of the flux between the direct and inverse energy cascades. The decrease in energy at high frequencies in the interval $0.397s < t < 1.3$ s is attributable to relaxation processes in the direct cascade. The corresponding redistribution of wave energy represents a sharing of the energy flux between the direct and inverse cascades, starting at about $t = 1.3$ s. The transient evolution shown in Figs. 3 (right) and 5 is incomplete: the forward and inverse energy fluxes are still changing at $t = 2s$, implying further relaxation oscillations at longer times (inaccessible with our present equipment): the transient dynamics is highly complex, and a full characterisation will require further work. For there to be a flux of energy towards low frequencies, there must be some dissipative mechanism there. We believe that it is probably attributable to viscous drag of the normal fluid component on the resonator walls, given that bulk second sound damping is negligibly small in this frequency range: this would be consistent with the observed strong decrease of the resonator Q-factor below 3 kHz. There is *hysteresis* between increasing and decreasing frequency scans (bars on data points in Fig. 6). The width of the hysteretic region, i.e. the region where the low frequency sound waves are metastable, was less than the viscous width of the resonance.

THEORY AND DISCUSSION

The use of a numerical technique has enabled us to gain a more detailed understanding of wave energy transformation in the acoustic turbulence regime [10]. It involves direct integration of the 2-fluid thermohydrodynamical equations [24], expanded up to quadratic terms in the wave amplitude. It represents the second sound waves in terms of Hamiltonian variables [9, 25], similar to the approach used in earlier studies [22] of acoustic turbulence. Wave damping was taken explicitly into account at all frequencies, however, a feature that is of key importance for a correct description of subharmonic generation. The main results are summarised in Fig. 6. To correspond with the experimental conditions, we assume full reflection of the waves from the resonator boundaries, rather than periodic boundary conditions [22].

It is found that, for sufficiently high driving amplitude W, the wave develops an instability with respect to generation of low-frequency subharmonics of the driving force
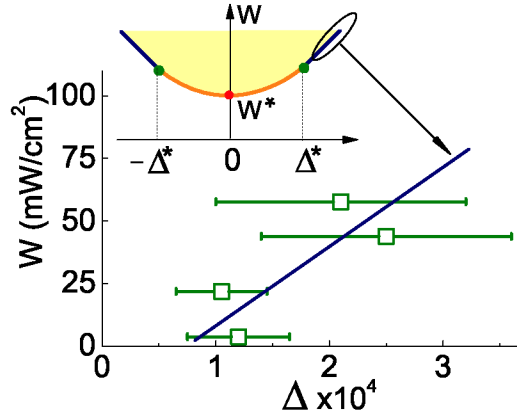
FIGURE 6. Dependence of the AC heat flux density W at which the instability develops on the dimensionless frequency detuning $\Delta = (\omega_d - \omega_n)/\omega_n$ of the driving force frequency ω_d from a cavity resonance ω_n. Numerical calculations (line) are compared with measurements (points) for driving at the 96th resonance. Horizontal bars mark the widths of the hysteretic region where second sound exists in a metastable state. Inset: bifurcation diagram showing regions of stability (unshaded) and regions of instability (yellow shaded) against the generation of subharmonics. The soft instability occurs over the (orange) line between the (green) critical points at $\pm\Delta^*$; outside them lies the hard instability; W^* is the threshold value of the instability. From [10]

at ω_d: see inset of Fig. 6. For zero detuning from a cavity resonance, the onset of the instability occurs at a threshold $W^* \propto 1/\alpha$. If the dimensionless frequency detuning $|\Delta|$ is less than a critical value $\Delta^* \sim 1/Q$, the instability has a soft character, in that the amplitudes of the low frequency waves tend to zero at the threshold bifurcation line. Outside this range, the low frequency waves are characterised by the hard onset observed experimentally. Measurements (squares) are compared with theory (full line) in the main part of Fig. 6. The hard onset is accompanied by a finite jump in subharmonic amplitude. These two regimes of behaviour are separated by critical points on the bifurcation line. The generation of subharmonics in the nonlinear oscillatory system found numerically appears to be similar to the bifurcation of an anharmonic oscillator [26]. The estimated value of the critical detuning parameter Δ^* at $T = 2.08$ K is close to 10^{-4}, and and that of the critical AC heat flux density W^* is equal to a few mW/cm^2, in good agreement with the observations. The results of Fig. 2 can be understood as corresponding to the working point moving horizontally on the bifurcation diagram (Fig. 6, inset) into the (yellow) shaded region from a position just outside it, through the hard (blue) instability line. Nonlocal (in ω-space) interactions between waves at ω_d and low frequency waves probably contributes to the subharmonics, due to the finite width of the low-frequency spectral domain, but we estimate that the interactions of high-frequency ($\omega \gg \omega_d$) waves with subharmonics are relatively weak, consistent with our inference of two cascades.

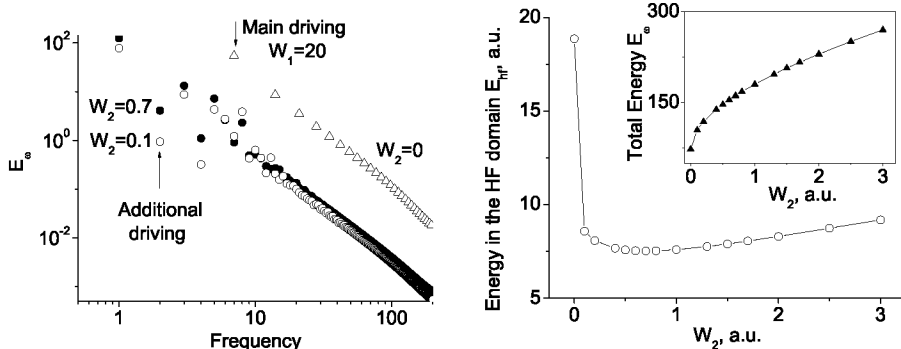The numerical calculations can also encompass the main effects of double-driving.

60

FIGURE 7. Effect of a weak secondary forcing. The left panel plots the stationary power spectra with the secondary drive amplitude $W_2 = 0$ (triangles) and for two nonzero values of W_2 (filled and open circles). The right panel plots as functions of W_2 in arbitrary units the energy in the high frequency domain and (inset) the total energy.

Fig. 7 illustrates the calculated effect of applying a weak additional driving force. The left-hand panel shows how the spectra are modified by application of a lower-frequency secondary forcing at amplitudes W_2 that are 10% and 70% of the main drive. There is dramatic decrease in the energy flux to the high frequency domain. The effect is quite insensitive to the amplitude of the secondary drive. The dramatic changes are shown explicitly in the right-hand panel. At the same time, the total turbulent wave energy increases monotonically with W_2. It is evident (left-hand panel) that the secondary forcing has triggered the inverse cascade, causing the onset of an energy flux towards the low-frequency domain. This latter effect has not yet been observed experimentally.

A physically intuitive explanation of these phenomena is that the additional forcing effectively relaxes the conservation laws governing the nonlinear wave transformations, and thus opens up many more channels via which the frequency-changing interactions can occur.

CONCLUSIONS

These experiments described above have revealed an inverse wave energy cascade in a turbulent acoustic system. It is responsible for a substantial increase in wave amplitude and for the formation of high-amplitude, low-frequency, subharmonics. The instability develops through formation of isolated low-frequency waves of higher amplitude than is typical of the waves around them. The higher-amplitude lone waves can be considered as the acoustic analogue of the giant "rogue" waves that occasionally appear on the ocean and endanger shipping. Their origin lies in a decay instability of the periodic wave, i.e. a similar mechanism to that proposed [27, 11] (modulation instability) to account for the creation of oceanic rogue waves [28].

ACKNOWLEDGEMENTS

REFERENCES

1. A. N. Kolmogorov, *Dokl. Akad. Nauk. SSSR* **30**, 299–303 (1941).
2. V. E. Zakharov, G. Falkovich, and V. S. L'vov, *Kolmogorov Spectra of Turbulence I*, Springer, Berlin, 1992.
3. J. P. Richter, *The Notebooks of Leonardo da Vinci*, Dover, New York, 1970.
4. J. L. Lumley, *Phys. Fluids A* **4**, 203–211 (1992).
5. V. S. Tsoi, *CEJP* **1**, 72–90 (2003).
6. S. N. Gurbatov, V. V. Kurin, L. M. Kustov, and N. V. Pronchatov-Rubtsov, *Acoust. Phys.* **51**, 152–159 (2005).
7. G. S. Bisnovatyi-Kogan, and S. A. Silich, *Rev. Mod. Phys.* **67**, 661–712 (1995).
8. M. Ryutova, and T. Tarbell, *Phys. Rev. Lett.* **90**, 191101 (2003).
9. G. V. Kolmakov, V. B. Efimov, A. N. Ganshin, P. V. E. McClintock, and L. P. Mezhov-Deglin, *Phys. Rev. Lett.* **97**, 155301 (2006).
10. A. N. Ganshin, V. B. Efimov, G. V. Kolmakov, L. P. Mezhov-Deglin, and P. V. E. McClintock, *Phys. Rev. Lett.* **101**, 065303 (2008).
11. A. I. Dyachenko, and V. E. Zakharov, *JETP Lett.* **81**, 255–259 (2005).
12. D. R. Solli, C. Ropers, P. Koonath, and B. Jalali, *Nature* **450**, 1054 (2007).
13. P. W. Anderson, and H. Suhl, *Phys. Rev.* **100**, 1788 (1955).
14. V. S. L'vov, *Wave Turbulence under Parametric Excitation. Application to Magnetics*, Springer, Berlin, 1994.
15. T. Matsushita, R. Nomura, H. H. Hensley, H. Shiga, and T. Mizusaki, *J. Low Temp. Phys.* **105**, 67–92 (1996).
16. S. R. Spangler, J. A. Leckband, and I. H. Cairns, *Phys. Plasmas* **4**, 846–855 (1997).
17. D. Rinberg, V. Cherepanov, and V. Steinberg, *Phys. Rev. Lett.* **76**, 2105–2108 (1996).
18. J. Wilks, *The Properties of Liquid and Solid Helium*, Clarendon Press, Oxford, 1967.
19. A. J. Dessler, and W. H. Fairbank, *Phys. Rev.* **104**, 6–12 (1956).
20. V. B. Efimov, A. N. Ganshin, P. V. E. McClintock, G. V. Kolmakov, and L. P. Mezhov-Deglin, *J. Low Temp. Phys.* **145**, 155–164 (2006).
21. H. Davydowitz, Y. L'vov, and V. Steinberg, *Physica D* **84**, 635 (1995).
22. G. Falkovich, and M. Meyer, *Phys. Rev. E* **54**, 4431–4434 (1996).
23. P. V. E. McCintock, V. B. Efimov, A. N. Ganshin, , G. V. Kolmakov, and L. P. Mezhov-Deglin, *J. Low Temp. Phys.* **150**, 394–401 (2008).
24. L. D. Landau, and E. M. Lifshitz, *Fluid Mechanics*, Butterworth and Heinemann, Oxford, 1987.
25. V. L. Pokrovskii, and I. M. Khalatnikov, *Sov. Phys. JETP* **44**, 1036 (1976).
26. L. Mandelstam, and N. Papalexi, *Z. Phys.* **73**, 223–248 (1932).
27. M. Onorato, A. R. Osborne, M. Serio, and S. Bertone, *Phys. Rev. Lett.* **86**, 5831–5834 (2001).
28. R. G. Dean, "Freak waves: a possible explanation," in *Water Wave Kinetics*, edited by A. Torum, and O. T. Gudmestad, Kluwer, Amsterdam, 1990, p. 609.